iScience

CellPress
OPEN ACCESS

Article

Prototype fabrication and performance evaluation of a thermoelectric module operating with the Nernst effect

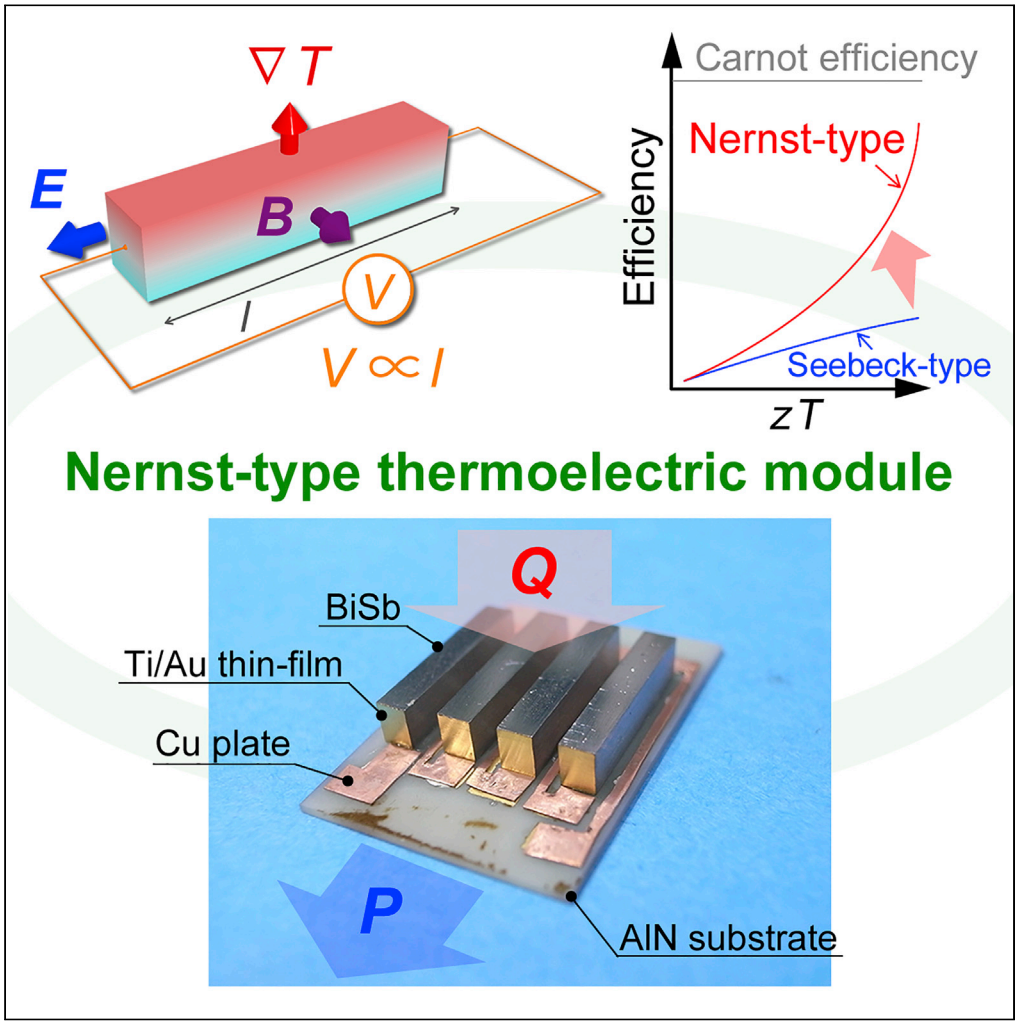

Masayuki Murata, Kazuo Nagase, Kayo Aoyama, Atsushi Yamamoto, Yuya Sakuraba

m.murata@aist.go.jp

Highlights

Thermoelectric module operating with the Nernst effect is developed as a prototype

Power density of 86.7 μW/cm^2 is obtained with a temperature difference of 149 K

Temperature difference of 82 mK occurs as a cooling operation

Murata et al., iScience 24, 101967
January 22, 2021
https://doi.org/10.1016/j.isci.2020.101967

iScience

CellPress
OPEN ACCESS

Article

Prototype fabrication and performance evaluation of a thermoelectric module operating with the Nernst effect

Masayuki Murata,[1,3,*] Kazuo Nagase,[1] Kayo Aoyama,[1] Atsushi Yamamoto,[1] and Yuya Sakuraba[2]

Summary

The Nernst effect generates a voltage transverse to the temperature gradient in the magnetic field. Although the Nernst effect has the potential to realize novel devices in the field of thermoelectric generators and sensors, thermoelectric modules that operate with the Nernst effect have not yet been implemented. Therefore, in this study, a thermoelectric module utilizing the Nernst effect was developed as a prototype, and its performance was evaluated to identify technical issues. The proposed module is fabricated by arranging four rectangular bars of a BiSb-based sintered alloy on an AlN substrate and connecting all the bars in series with Cu plates. As a result of the measurement, when the magnetic field was 5 T, an output power of 0.48 mW was obtained with a temperature difference of 149 K, and a temperature difference of 82 mK occurred as a cooling operation with an applied electrical current of 100 mA.

Introduction

High-efficiency energy conversion techniques utilizing the thermoelectric effect, which aim at energy harvesting devices for Internet of things power sources, are being actively studied in a wide range of research fields. Our research group has also extensively studied the thermoelectric effect, focusing on both basic research and practical applications, including nanoscale materials, bulk materials, and module development and evaluation (Ohta et al., 2019). Recent studies have reported a high energy conversion efficiency of 12% on the cascade-type module, which is derived from the high dimensionless figure of merit $zT \sim 1.9$ of PbTe-based alloys (Jood et al., 2018). The conversion efficiency is gradually increasing with active research; however, power generation using the Seebeck effect essentially suppresses the enhancement of the conversion efficiency owing to the heat flow caused by the Peltier effect in the same direction as that of Fourier 's law (Nolas et al., 2001). When the thermoelectric modules operate under the temperature difference, both the Seebeck effect and the Peltier effect occur simultaneously because the electrical current flows through the module owing to the load resistance connected to the module for practical power generation operation. In contrast, it has been suggested that power generation by the Nernst effect can achieve extremely high conversion efficiency (Harman and Honig, 1967). The Nernst effect generates a voltage transverse to the temperature gradient and magnetic field, and conversely, the Ettingshausen effect generates a temperature difference transverse to the electrical current and magnetic field. For power generation using the Nernst effect, the direction of the heat flow induced by the Ettingshausen effect is opposite to that of the heat flow due to Fourier 's law, and the energy conversion efficiency is enhanced by this phenomenon (Yamaguchi, 2002). In addition, the coefficient of performance for the cooling operation of the Ettingshausen effect is expected to be significantly improved as compared with that of the Peltier effect due to a similar mechanism.

Furthermore, the module configuration using the Nernst effect is more simplified compared with that using the Seebeck effect because an electric field is generated perpendicular to the temperature gradient, and the voltage increases proportionally with the increase in the bar length along the electric field (Norwood, 1963). This implies that the Π-type structure generally used for modules operating with the Seebeck effect is not required for modules operating with the Nernst effect, and the Nernst-type thermoelectric module can be realized by material having one sign Nernst coefficient. Although an external magnetic field is required to obtain the thermoelectromotive force by the Nernst effect, using the current technology, a magnetic field of 1 T can be easily achieved using a powerful permanent magnet such as a neodymium magnet. Although the volume of the module is increased by incorporating permanent magnets,

[1]Research Institute for Energy Conservation, National Institute of Advanced Industrial Science and Technology (AIST), 1-1-1 Umezono, Tsukuba, Ibaraki 305-8568, Japan

[2]Research Center for Magnetic and Spintronic Materials, National Institute for Materials Science (NIMS), 1-2-1 Sengen, Tsukuba, Ibaraki 305-0047, Japan

[3]Lead contact

*Correspondence: m.murata@aist.go.jp

https://doi.org/10.1016/j.isci.2020.101967

thermoelectric conversion with high conversion efficiency can be realized in a place where the installation area is not limited. Furthermore, a new concept of a thermoelectric module operating with the anomalous Nernst effect (ANE) has been recently reported using ferromagnets, which can occur by an internal magnetic field instead of an external magnetic field (Sakuraba, 2016). Thermoelectric modules operating with ANE have many advantages in energy harvesting devices requiring mass production because they gain the above mentioned benefits without applying an external magnetic field. Although the thermopower of ANE has been insufficient for practical use in the past, it has been rising and reaching ~6 μV/K because of recent active research (Mizuguchi et al., 2012; Sakuraba et al., 2013; Nakatsuji et al., 2015; Kim et al., 2016; Reichlova et al., 2018; Nakayama et al., 2019; Guin et al., 2019; Sakai et al., 2020). Furthermore, the power-generating characteristics of a spiral structure thermoelectric module operating with the Nernst effect, using a coiled galfenol wire, has also been reported (Yang et al., 2017). As mentioned above, the Nernst effect and modules on ferromagnetic materials have been extensively studied recently. On the other hand, long known thermoelectric materials such as Bi and BiSb show a large Nernst thermopower of several hundred $\mu V\ K^{-1}$ (Harman et al., 1964). Its origin is the extraordinarily high mobility of electrons and low Fermi energy (Behnia, 2009). In addition, a large Nernst coefficient has also been reported using other high-carrier mobility materials such as InSb ($-82\ \mu V\ K^{-1}\ T^{-1}$ at 283 K) (Nakamura et al., 1997), Ge ($320\ \mu V\ K^{-1}\ T^{-1}$ at 360 K) (Mette et al., 1959), and Cd_3As_2 ($107\ \mu V\ K^{-1}\ T^{-1}$ at 250 K) (Xiang et al., 2020). However, a thermoelectric module using these materials operating with the Nernst effect has not been reported. Most studies on the Nernst effect of these materials have focused on the evaluation of basic physical properties in the low-temperature range (Wang et al., 2006; Behnia et al., 2007; Nakamura et al., 2005) and are not intended for power generation applications (Angrist, 1963). Therefore, in this research, a prototype thermoelectric module operating with the Nernst effect is fabricated using a BiSb sintered alloy, which has a high Nernst coefficient. The power generation and cooling performance of the developed Nernst-type thermoelectric module are evaluated to clarify the technical issues of the module. The fabrication and evaluation method of the Nernst-type thermoelectric module elucidated in this study is expected to be applied to thermoelectric modules that operate not only with the normal Nernst effect but also with ANE.

Results

In the thermoelectric module operating with the Seebeck effect, it is necessary to connect several thermoelectric materials in series to increase the output voltage because an electric field is generated parallel to the temperature gradient, as shown in Figure 1A. In general, commercially available thermoelectric modules are manufactured by assembling many Π-type structures consisting of a pair of n-type and p-type carrier materials (Nolas et al., 2001). In a typical Seebeck-type module, the output voltage is proportional to the number of thermoelectric legs when the temperature difference is constant. Hence, it is necessary to construct a module using a complicated structure with many electrical and thermal junctions between the electrodes and the materials that suppress the performance of the module. In contrast, the thermoelectric module operating with the Nernst effect can be realized with much fewer junctions, as shown in Figure 1B, because the output voltage increases with an increase in the length l of the material. In addition, the pair of n-type and p-type carrier materials, which is required for the Seebeck-type thermoelectric module, is not required for the Nernst-type thermoelectric module. The Nernst-type thermoelectric module can be constructed by a unileg-like structure placed perpendicular to the temperature difference using a metal circuit on the substrate. The energy conversion efficiency is not reduced by the heat loss through the metal circuit, as it occurs in a conventional unileg structure of the Seebeck-type modules because the metal circuit formed on the substrate does not pass heat flow from the hot side to the cold side. Moreover, it is also possible to form the Π-type structure for the Nernst-type module by controlling the sign of the Nernst coefficient that is not determined by the carrier type but by the carrier scattering mechanism (Jin and Heremans, 2018; Arisaka et al., 2018).

The output voltage and internal resistance of the module increases in proportion to the number of materials n (the material's length l) on the Seebeck-type module (the Nernst-type module), as shown on the left axis of Figure 1C. The internal resistance of the module can be reduced by increasing the cross-sectional area where electrical current flows, that is, increasing the material width w or depth d (height h or depth d) for the Seebeck-type module (the Nernst-type module). However, the output voltage decreases by increasing the height of the Nernst-type module because the Nernst thermopower is not determined by the temperature difference but by the temperature gradient unlike that of the Seebeck effect. Therefore, to control the internal resistance of the Nernst-type module applied to a heat source with a constant temperature difference, it is appropriate to change the material depth to maintain the output voltage. The optimal module, which shows the maximum energy conversion efficiency, is designed by matching the

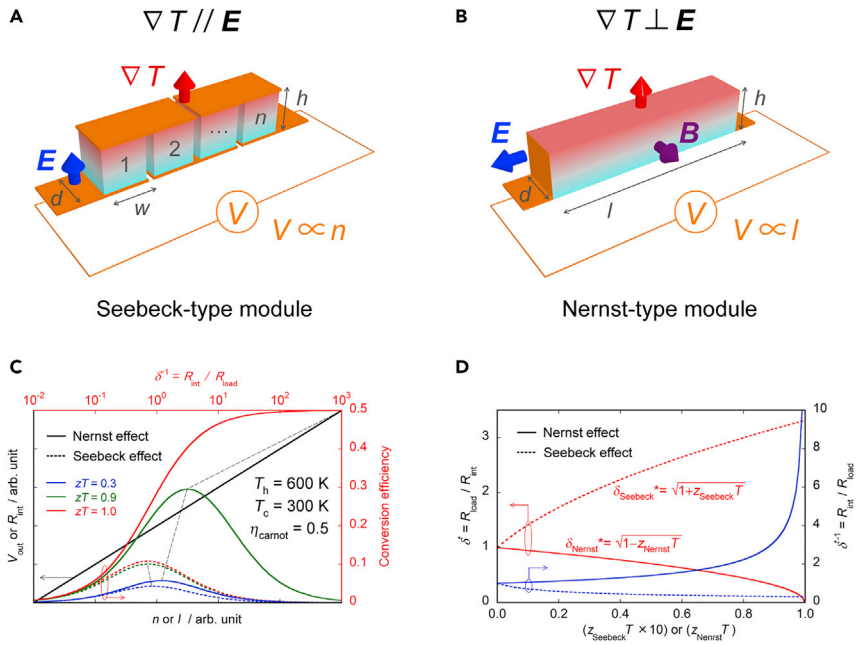

Figure 1. Comparison of the Seebeck-type and Nernst-type thermoelectric modules

(A and B) Configurations of the thermoelectric module operating with (A) the Seebeck effect and (B) the Nernst effect.

(C) The number of material (material's length) dependence of the output voltage or internal resistance of the Seebeck-type module (the Nernst-type module) on the left y axis, and the inverse resistance ratio dependence of the energy conversion efficiency of the Seebeck effect (dashed line) and Nernst effect (solid line) on the right y axis.

(D) zT dependence of the optimal resistance ratio on the left axis and those reciprocals on the right axis.

internal resistance of the module with the load resistance. The ratio of the load resistance and internal resistance to obtain maximum energy conversion efficiency differs between the Seebeck-type and Nernst-type modules. The energy conversion efficiency of the Seebeck effect $\eta_{Seebeck}$ and the Nernst effect η_{Nernst} as a function of the resistance ratio of the load resistance and the internal resistance δ ($=R_{load}/R_{int}$) is expressed by (Harman and Honig, 1967):

$$\eta_{Seebeck} = \frac{T_h - T_c}{T_h}\left(\frac{\frac{\delta}{1+\delta}}{\frac{1}{z_{Seebeck}}\frac{1+\delta}{T_h} - \frac{1}{2}\frac{T_h - T_c}{T_h}\frac{1}{1+\delta} + 1}\right) \quad \text{(Equation 1)}$$

$$\eta_{Nernst} = \frac{T_h - T_c}{T_h}\left(\frac{\frac{\delta}{1+\delta}}{\frac{1}{z_{Nernst}}\frac{1+\delta}{T_h} - \frac{1}{2}\frac{T_h - T_c}{T_h}\frac{1}{1+\delta} - \frac{T_c}{T_h}}\right) \quad \text{(Equation 2)}$$

where T_h and T_c are the hot side and cold side temperatures, respectively, and the figure of merit of the Seebeck effect $z_{Seebeck}$ and the Nernst effect z_{Nernst} is defined as follows:

$$z_{Seebeck} = \frac{S^2}{\rho\,\kappa} \quad \text{(Equation 3)}$$

$$z_{Nernst} = \frac{(NB)^2}{\rho\,\kappa} \quad \text{(Equation 4)}$$

where S, N, B, ρ, and κ are the Seebeck coefficient, Nernst coefficient, magnetic field, electrical resistivity, and thermal conductivity, respectively. The inverse resistance ratio dependence of the energy conversion efficiency of the Seebeck effect (dashed line) and Nernst effect (solid line) considering $z_{Seebeck}T$ and $z_{Nernst}T$ = 0.3, 0.9, and 1.0 with the temperature conditions of T_h = 600 K, T_c = 300 K, and $T = (T_h + T_c)/2$ is shown on the right axis of Figure 1C. The energy conversion efficiency of both the Seebeck effect and Nernst effect increases with zT, and the efficiency of the Nernst effect increases much more than that of the Seebeck effect. Furthermore, the inverse resistance ratio to obtain the maximum energy conversion

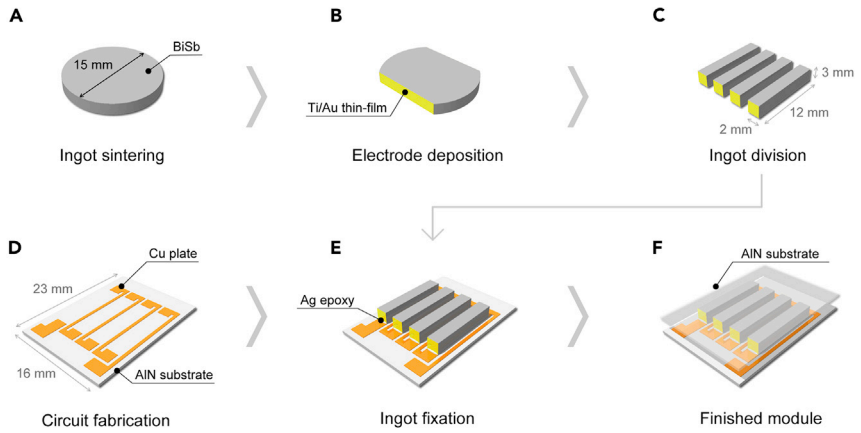

Figure 2. Schematic diagram of the fabrication procedure on the Nernst-type thermoelectric module

(A) BiSb alloy ingot sintering.

(B) Cutting off the ingot and Ti/Au electrode deposition.

(C–F) (C) Division into four rectangular bars, (D) Cu circuit fabrication on the AlN substrate, (E) bar fixation on the substrate and electrical contact, and (F) finished module by attaching the AlN substrate to the bars.

efficiency of the Seebeck effect decreases with $z_{Seebeck}T$, while the inverse resistance ratio on the Nernst effect increases with $z_{Nernst}T$. In Figure 1D, the zT dependence of the optimal resistance ratio $\delta^*_{Seebeck}$, δ^*_{Nernst} on the left axis, and those reciprocals on the right axis calculated from (Harman and Honig, 1967) are shown.

$$\delta^*_{Seebeck} = \sqrt{1 + z_{Seebeck}T} \quad \text{(Equation 5)}$$

$$\delta^*_{Nernst} = \sqrt{1 - z_{Nernst}T} \quad \text{(Equation 6)}$$

These dependences also indicate that the optimal resistance ratio of the Seebeck effect increases with $z_{Seebeck}T$, while that of the Nernst effect decreases with $z_{Nernst}T$. In other words, the internal resistance of the Nernst-type module must be large with increasing $z_{Nernst}T$, and this is favorable because the internal resistance of the Nernst-type module increases with the material length to increase the output voltage.

A schematic diagram of the fabrication procedure of the Nernst-type thermoelectric module is shown in Figure 2. First, a disk-shaped ingot of a BiSb-based alloy with a diameter of 15 mm and a thickness of 3 mm (Figure 2A) was prepared as described in Supplemental Information. Next, two parts of the ingot were cut in parallel, as shown in Figure 2B, and Ti (10-nm-thick) and Au (100-nm-thick) thin films on cut facets were formed using the vacuum vapor deposition method (Eiko Engineering EB-680). In addition, the ingot was divided into four bars of a rectangular parallelepiped with dimensions of 12 × 2 × 3 mm^3 (Figure 2C). Meanwhile, two AlN substrates with a thickness of 0.4 mm and an area of 16 × 23 mm^2 (Furukawa Denshi FAN-170) were prepared using a dicing saw (Disco DAD522) for use as the ceramic plate of the module. An electrical circuit made of 0.1-mm-thick Cu plates was placed on one AlN substrate using Ag epoxy (Diemat Sk100SDN), as shown in Figure 2D. Subsequently, the four bars of the rectangular parallelepiped were arranged on the AlN substrate using a silicone adhesive (ThreeBond 1225B) and electrically connected using Ag epoxy (Figure 2E). The module was heated at 150°C for 30 min using a hot plate to cure Ag epoxy, and it was previously confirmed that this curing temperature and time do not affect the measurement results of the thermoelectric properties of BiSb alloys. Although the Nernst effect can cause the voltage to be proportional to the length of the bar, the series connection of several bars is required to place bars in a practical square area of the module. Finally, the Nernst-type thermoelectric module was completed by fixing the AlN substrate of the same dimensions as the lower substrate directly to the upper face of the bars using the adhesive, as shown in Figure 2F.

In Figure 3A, an image of the Nernst-type thermoelectric module after arranging four bars on the AlN substrate is depicted. The completed module was placed on a heat sink made of Cu such that the magnetic field can be applied in plane of the module and perpendicular to the longitudinal direction of the bars, as shown in Figures 3B–3D. A 1000-W rated ceramic heater with a 25 × 25 mm square shape was attached on the hot side of the module and secured using a nylon tie. Thermal contacts between the module and heat sink and between the module and ceramic heater were obtained by vacuum grease (Apiezon N

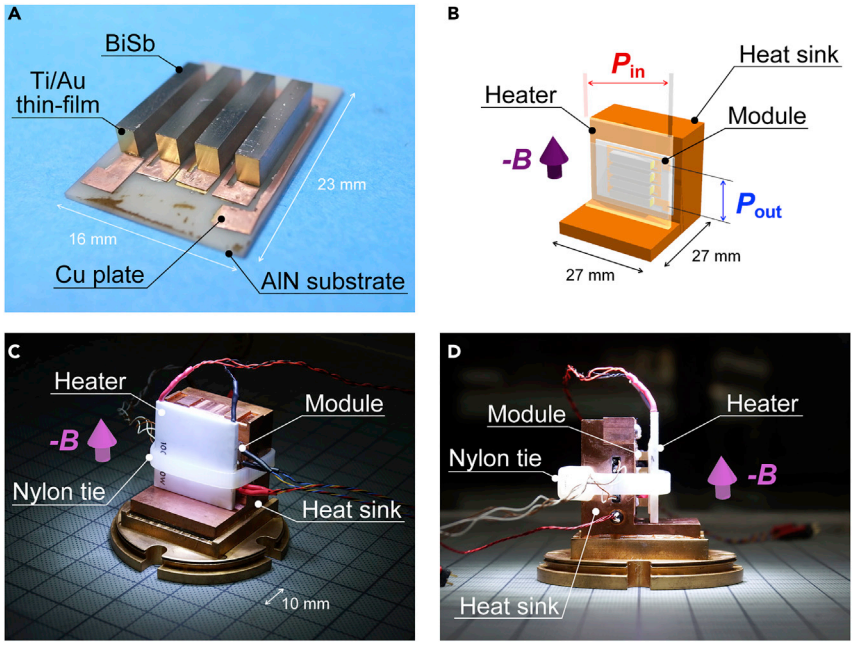

Figure 3. Photographs and 3D schematic diagram of the fabricated module and measurement setup

(A) Photograph of the Nernst-type module after attaching four bars.

(B) Schematic of the measurement setup.

(C and D) Photographs of the measurement setup with (C) a bird's-eye view and (D) side view.

Grease). The two lead wires for electrical current and voltage were electrically connected to both the positive and negative electrodes of the module by Ag epoxy to evaluate the module using the four-wire method. A type-T differential thermocouple was attached to the hot and cold sides of the AlN substrates inside the module to measure the temperature difference. The heat sink on which the module was placed was attached to the cryohead of the Gifford-McMahon refrigerator (Sumitomo Heavy Industries RDK-415D) of the cryostat equipped with a superconducting magnet, and subsequently, the chamber was evacuated to less than 10^{-3} Pa. The schematic configuration of the measurement system of the Nernst-type thermoelectric module is described in Supplemental information.

In Figure 4A, the measured magnetic field dependence of the output voltage on the Nernst-type module when the load current is varied from −40 mA to +70 mA in 10-mA intervals is shown. The cold side temperature of the module was controlled at 273.15 K, and the temperature difference induced in the module was 133 K in the absence of the magnetic field and increased with the increase in the absolute value of the magnetic field, as depicted on the right axis of Figure 4D. The open-circuit voltage, with a curve of 0 mA load current, was 3.2 mV at 0 T and increased with the positive magnetic field to a maximum value of 27.2 mV at approximately 4.8 T and decreased with the negative magnetic field to a minimum value of −17.5 mV at approximately −3.9 T. The sign of the output voltage for positive and negative magnetic fields is the opposite because the Nernst thermopower is an odd function of the magnetic field. The Nernst voltage must be zero in the absence of the magnetic field; however, the output voltage is not zero at 0 T, which is brought about by the Seebeck effect, which is generated by the temperature distribution in the in-plane direction of the Nernst-type module. In addition, the absolute values of the maximum and minimum voltages for the positive and negative magnetic fields did not match, even though the Nernst voltage was an odd function. The output voltage of the Nernst-type module produced in this study shows the summation of the two thermoelectromotive forces of the Nernst effect and the Seebeck effect. The contributions of the Nernst effect and Seebeck effect on the output voltage could be separated by considering that the Nernst thermopower is an odd function and the Seebeck thermopower is an even function using the open circuit voltage, as shown in Figure 4B. The pure output voltage component derived from the Nernst effect was 22.2 mV at 5 T and the offset voltage was 5.0 mV. The offset voltage increased from 3.2 mV to 5.0 mV when the absolute value of the magnetic field increased from 0 T to 5 T because the Seebeck coefficient varies with an even function of the magnetic field, which is known as the magneto-Seebeck effect (Wolfe and Smith, 1962). The module output voltage was saturated in the high

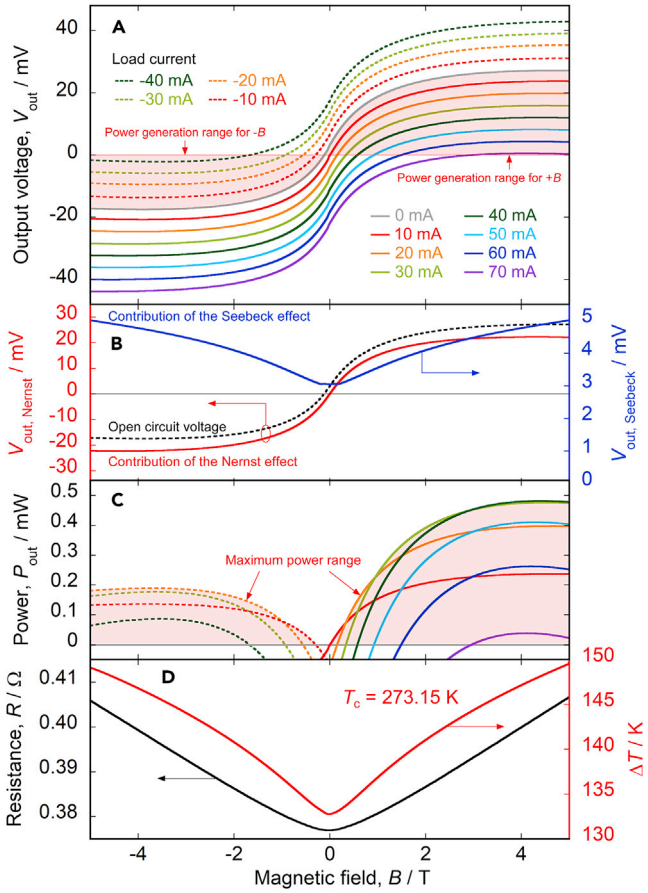

Figure 4. Measurement results of the Nernst-type thermoelectric module

Magnetic field dependences of (A) the output voltage on the Nernst-type module with a load current from −40 mA to +70 mA, (B) the contributions of the Nernst effect and Seebeck effect to the output voltage, (C) output power for all load currents, and (D) internal resistance of the module on the left y axis and the temperature difference induced in the module when the load current is 0 mA on the right y axis.

magnetic field because the Nernst thermopower of the Te-doped BiSb is saturated at a higher magnetic field (Murata et al., 2020). The range of the power-generating operation is shown in Figure 4A. As observed in the figure, the positive output voltage has a positive load current in the positive magnetic field, and the negative output voltage has a negative load current in the negative magnetic field.

The magnetic field dependence of the module output power for all load currents calculated by multiplying the output voltage by the load current is shown in Figure 4C. The maximum output power was increased in both the positive and negative magnetic fields, and the difference between the maximum power in the positive and negative magnetic fields was caused by the Seebeck effect. The local maximum power for the positive magnetic field was 0.48 mW at a load current of 40 mA at 4.4 T, whereas the local maximum power for the negative magnetic field was 0.19 mW at a load current of −20 mA at −3.7 T. The magnetic field dependence of the internal resistance of the module at 273.15 K on the left y axis and the temperature difference induced in the module when the load current is 0 mA on the right y axis are shown in Figure 4D. The internal resistance increased from 377 mΩ to 406 mΩ in the magnetic field from 0 T to 5 T, which is caused by the large magneto-resistance effect of the BiSb alloy even in the room temperature range. The temperature difference of the module increased from 133 K to 149 K in the magnetic field from 0 to 5 T due to a reduction in the electron thermal conductivity caused by the increase in the electrical resistance. The contribution of only four bars to the internal resistance of the module estimated from the measured electrical resistivity of the Te-doped $Bi_{88}Sb_{12}$ alloy and the bar dimension was 26.4 mΩ at 5 T, and the measured internal resistance of the module was approximately 15 times larger than the material resistance. The contribution of the contact resistance was estimated to be 380 mΩ, which could be caused by Ag epoxy between the

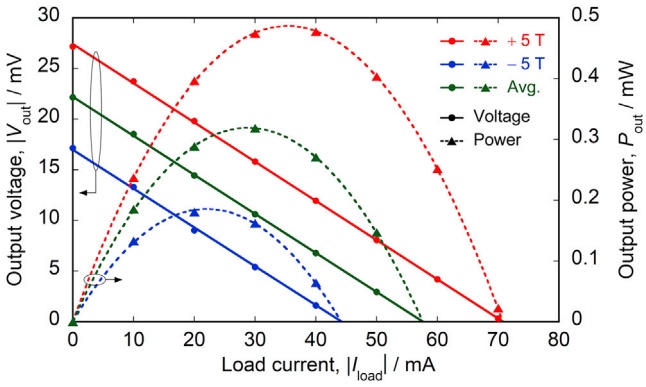

Figure 5. Output voltage and power of the Nernst-type module as a function of the absolute value of the load current in a magnetic field of ±5 T and averaged values at ±5 T

elements and Cu electrical circuits. There are other options for obtaining lower electrical contact resistance, such as solder and Wood's metal; however, they easily form eutectic with BiSb alloys. The Nernst thermopower of contaminated BiSb alloys is reduced because the Nernst effect is significantly sensitive to impurities and scattering mechanisms (Arisaka et al., 2018). Ag epoxy was not the best choice, but it was used to produce the Nernst-type module prototype because the purpose of this study is to prove the operation and reveal technical issues. On the other hand, the thermal conductivity of the BiSb alloy is estimated to be 2.3 W/mK at 5 T using the heater power, temperature difference, and dimensions of the elements of the produced module. This is less than the measured thermal conductivity of 2.7 W/mK using the single bar-shaped ingot at 5 T and 300 K, as shown in Figure S2B, owing to the thermal contact resistance between ceramic substrates and elements. Although the temperature regions for determining these two thermal conductivities were different, the thermal conductivity estimated by the module was smaller than the material value even considering that the thermal conductivity of BiSb alloy shows the positive temperature coefficient around 300 K (Lenoir et al., 1995). The contribution of the Seebeck effect to the output voltage shown in Figure 4B also implies that thermal contacts between the elements and ceramic substrates were not uniform. The thermal contact resistance can be reduced by exploring suitable adhesive and making elements of the same height with high precision to obtain good contact.

In Figure 5, the output voltage and power of the Nernst-type module as a function of the absolute value of the load current in a magnetic field of ±5 T are shown. The open-circuit voltages were 27.4 mV and −17.0 mV, the short-circuit currents were 70.9 mA and −44.3 mA, the maximum powers were 0.487 mW and 0.186 mW, and the optimum load currents were 35.4 mA and −22.1 mA, respectively, in the magnetic field of 5 T and −5 T. The maximum power in the positive magnetic field was 2.6 times greater than that in the negative magnetic field owing to the Seebeck effect as explained above. The averaged voltage and the power of the values of ±5 T, which are a pure contribution of the Nernst effect, are also plotted in the same graph. The open-circuit voltage, short-circuit current, maximum power, and optimum load current of the module considering only the influence of the Nernst effect are 22.2 mV, 57.6 mA, 0.319 mW, and 28.8 mA, respectively. The uncertainty of the output power was small enough because it was determined by the electrical current input using the current source and the voltage measured using the digital multimeter (DMM). The measurement error of the output voltage evaluated from the I-V curve in Figure 5 was 0.1 mV, which led to a measurement error of the maximum output power to be 0.003 mW. Considering that the area of the fabricated module was 16 × 23 mm^2, the power density per unit area was calculated to be 86.7 μW cm^{-2}.

The heat flow passing through the Nernst-type thermoelectric module can be estimated from the heater power, assuming that the heat leakage from the nylon tie and heater wires is negligible. The applied heater power was calculated to be 11.2 W with an electrical current of 0.284 A and a voltage of 39.5 V, and the maximum output power from the module was 0.319 mW at 5 T, resulting in an energy conversion efficiency of 0.0028%. Here, the heat leakage from the nylon tie and ceramic heater leads can be estimated to be 1% of the heat flow through the module, considering the thermal conductivity of each material and the configuration of the evaluation setup shown in Figures 3C and 3D. In addition, the heat leakage due to the radiation from the ceramic heater was estimated to be ~1% of the heat flow through the module, which means that the heat flow through the module determined by the input current and voltage can be overestimated

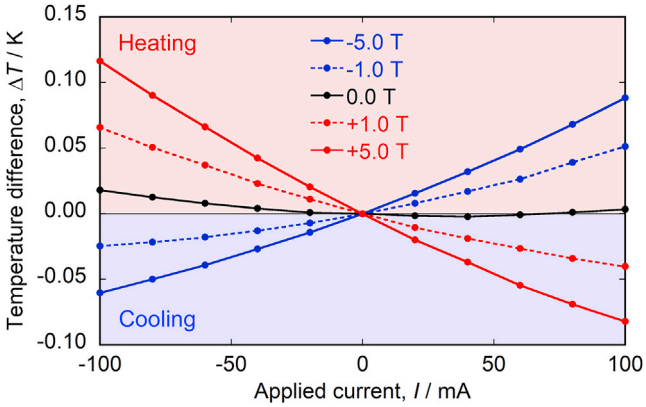

Figure 6. Dependence of the temperature difference caused by the Ettingshausen effect measured on the Nernst-type thermoelectric module in a magnetic field of 0 T, ±1 T, and ±5 T

by ~2%. As a result, the determined conversion efficiency could be underestimated by ~2% due to heat leakage and have an uncertainty of ~1% due to power measurement error. Here, the conversion efficiency was calculated by considering only the input heat flow to the module and the output electric power from the module in order to focus on the relationship between the figure of merit of the material and the energy conversion efficiency. The electrical energy required to apply the magnetic field was not included to calculate the efficiency because the energy loss on a superconducting coil is ideally zero. Although power is consumed by the current source and the refrigerator for the superconducting magnet, the power consumption of the equipment such as the current source and chiller is generally not included in the efficiency even in the evaluation of Seebeck-type thermoelectric modules (Ohta et al., 2019). Furthermore, the fabrication and evaluation technique of the Nernst-type thermoelectric module established in this study can be applied to modules operating with ANE, which can occur by internal magnetization, meaning that the external magnetic field is not necessary. The dimensionless figure of merit for the Nernst effect $z_{Nernst}T$ can be estimated from the conversion efficiency using the following equation (Harman and Honig, 1967):

$$\eta_{Nernst} = \frac{T_h - T_c}{T_h}\left(\frac{1-\sqrt{1-z_{Nernst}T}}{1+(T_c/T_h)\sqrt{1-z_{Nernst}T}}\right) \quad \text{(Equation 7)}$$

$z_{Nernst}T$ is estimated to be 3×10^{-4} at 5 T from Equations 4 and 7 using the measured conversion efficiency, which is an order of magnitude smaller than the expected value of the sintered BiSb alloy caused by the large contact resistance to the materials.

The applied current dependence of the temperature difference caused by the Ettingshausen effect measured on the Nernst-type thermoelectric module in a magnetic field of 0 T, ±1 T, and ±5 T is shown in Figure 6. The negative temperature difference shown on the y axis represents the cooling operation of the module. Although a slight cooling phenomenon was observed at 0 T for the positive electrical current due to the Peltier effect, the temperature increased with the absolute value of the applied electrical current due to Joule heating. The cooling and heating phenomena caused by the Ettingshausen effect were clearly observed in the magnetic field, and the cooling and heating operations were successfully changed by the sign of the magnetic field. The temperature difference due to cooling operation increased with the applied current and the magnetic field, reaching −82 mK at 100 mA for 5 T and −60 mK at −100 mA for −5 T. Although the maximum temperature difference for cooling operation is expected to be shown with an applied electrical current higher than 100 mA, the current was up to 100 mA because of the current source limitation. However, the maximum temperature difference was roughly estimated to be −144 mK at a current of 289 mA by extrapolating the measurement curve of 5 T with a quadratic function. The temperature difference obtained by the Ettingshausen effect was less than one-thousandth of the temperature difference of 149 K applied from the outside in the power generation evaluation, meaning that the influence of the Ettingshausen effect on power generation could be ignored.

Discussion

As described above, we successfully fabricated a prototype of the Nernst-type thermoelectric module using the BiSb sintered alloy and evaluated the power generation and cooling performance of the module. The

Nernst-type module could be realized in a simple configuration with fewer electrical connections between the materials and electrodes than the typical configuration of the Seebeck-type modules. Furthermore, the hot and cold sides of the materials were attached directly to the ceramic substrates without the metal electrodes required for the Π-structure of the Seebeck-type module. Therefore, the configuration of the Nernst-type module is suitable for obtaining the maximum performance of materials because the electrical and thermal resistance between the materials and the electrodes can be reduced. The power generation performance of the fabricated module was successfully evaluated, and the energy conversion efficiency was estimated to be 0.003%. This efficiency results in a $z_{Nernst}T$ value of 3×10^{-4}, which is 0.3% of the value measured using the individual ingot cut from the same ingot as the Nernst-type module, although it cannot be simply compered because the temperatures were not the same. The main reason for the low $z_{Nernst}T$ value is the high contact resistance between materials and electric circuits rather than the module structure because the module structure basically retains the phenomenon of the Nernst effect. Therefore, the output power can be enhanced by reducing the contact resistance using solder or Wood's metal instead of Ag epoxy for electrical connections and by improving the thermal contact between the materials and ceramic substrates. However, $z_{Nernst}T$ is still low for obtaining high energy conversion efficiency due to the Nernst effect because the conversion efficiency of a device based on the Nernst effect starts to outperform obviously based on the Seebeck effect when $z_{Nernst}T > 0.4$ (Harman and Honig, 1967). Therefore, $z_{Nernst}T$ needs to be enhanced to obtain the advantages of the Nernst effect on the energy conversion efficiency. We will develop and evaluate materials to enhance $z_{Nernst}T$ by controlling the effective mass or carrier doping. In the future, the relationship between energy conversion efficiency and $z_{Nernst}T$ will be experimentally revealed to prove the potential to obtain a significantly high energy conversion efficiency using the Nernst effect.

Limitations of the study

A thermoelectric module operating with the Nernst effect was developed as a prototype, and its performance in terms of power generation and cooling in the magnetic field was evaluated. The Nernst-type module was realized with a simple configuration because the Nernst effect can generate a voltage transversal to the temperature difference and is proportional to the length of the material. Furthermore, the configuration of the proposed Nernst-type module is suitable for obtaining the maximum performance of the materials because the electrical and thermal resistance between the materials and electrodes can be reduced. The results of the module evaluation demonstrated that when the magnetic field was 5 T, an output power of 0.487 mW was obtained with a temperature difference of 149 K, and a temperature difference of 82 mK was obtained as a cooling operation with an applied electrical current of 100 mA. The $z_{Nernst}T$ needs to be enhanced to obtain the advantages of the Nernst effect on the energy conversion efficiency. The evaluation method of the module, as explained in this study, can prove the possibility of the significantly high performance predicted in the Nernst effect.

Resource availability

Lead contact

Further information and requests for resources and reagents should be directed to and will be fulfilled by the Lead Contact, Masayuki Murata (m.murata@aist.go.jp).

Materials availability

This study did not generate new unique materials.

Data and code availability

The data supporting the current study are available from the corresponding author on request.

Methods

All methods can be found in the accompanying Transparent methods supplemental file.

Supplemental information

Supplemental Information can be found online at https://doi.org/10.1016/j.isci.2020.101967.

Acknowledgments

The authors would like to thank Drs. Chul-Ho Lee and Michihiro Ohta of National Institute of Advanced Industrial Science and Technology (AIST) for their assistance in this research. This research is based on results obtained from a project commissioned by Mitou challenge 2050 of the Advanced Research Program for

Energy and Environmental Technologies of New Energy and Industrial Technology Development Organization (NEDO). This work was supported in part by a Japan Society for the Promotion of Science (JSPS) KAKENHI Early-Career Scientists Grant Number 19K15297, Japan Science and Technology Agency (JST)-Mirai Program Grant Number JPMJMI19A1, Japan.

Author contributions

M.M., K.N., and K.A. conducted the experiments on fabrication and measurement of the prototype thermoelectric module operating with the Nernst effect; M.M., A.Y., and Y.S. conceived the idea of the configuration of the module; M.M. designed the experiments and wrote the paper.

Declaration of interests

The authors declare no competing interests.

Received: September 9, 2020
Revised: November 23, 2020
Accepted: December 15, 2020
Published: January 22, 2021

References

Angrist, S.W. (1963). A Nernst effect power generator. J. Heat Transf. *85*, 41–48.

Arisaka, T., Otsuka, M., and Hasegawa, Y. (2018). Investigation of carrier scattering process in polycrystalline bulk bismuth at 300 K. J. Appl. Phys. *123*, 235107.

Behnia, K. (2009). The Nernst effect and the boundaries of the Fermi liquid picture. J. Phys. Condens. Matter *21*, 113101.

Behnia, K., Méasson, M.-A., and Kopelevich, Y. (2007). Oscillating nernst-ettingshausen effect in bismuth across the quantum limit. Phys. Rev. Lett. *98*, 166602.

Guin, S.N., Manna, K., Noky, J., Watzman, S.J., Fu, C., Kumar, N., Schnelle, W., Shekhar, C., Sun, Y., Gooth, J., et al. (2019). Anomalous Nernst effect beyond the magnetization scaling relation in the ferromagnetic Heusler compound Co_2MnGa. NPG Asia Mater. *11*, 16.

Harman, T.C., and Honig, J.M. (1967). Thermoelectric and Thermomagnetic Effects and Applications (McGraw-Hill).

Harman, T.C., Honig, J.M., Fischler, S., and Paladino, A.E. (1964). The Nernst-Ettingshausen energy conversion figure of merit for Bi and Bi-4% Sb alloys. Solid State Electron. *7*, 505–508.

Jin, H., and Heremans, J.P. (2018). Optimization of the figure of merit in $Bi_{100-x}Sb_x/Al_2O_3$ nanocomposites. Phys. Rev. Mater. *2*, 115401.

Jood, P., Ohta, M., Yamamoto, A., and Kanatzidis, M.G. (2018). Excessively doped PbTe with Ge-induced nanostructures enables high-efficiency thermoelectric modules. Joule *2*, 1339–1355.

Kim, D.J., Lee, K.D., Surabhi, S., Yoon, S.G., Jeong, J.R., and Park, B.G. (2016). Utilization of the antiferromagnetic IrMn electrode in spin thermoelectric devices and their beneficial hybrid for thermopiles. Adv. Funct. Mater. *26*, 5507–5514.

Lenoir, B., Cassart, M., Michenaud, J.P., Scherrer, H., and Scherrer, S. (1995). Transport properties of Bi-rich Bi-Sb alloys. J. Phys. Chem. Sol. *57*, 89–99.

Mette, H., Gärtner, W.W., and Loscoe, C. (1959). Nernst and ettingshausen effects in germanium between 300 and 750°K. Phys. Rev. *115*, 537–542.

Mizuguchi, M., Ohata, S., Uchida, K., Saitoh, E., and Takanashi, K. (2012). Anomalous Nernst effect in an $L1_0$-ordered epitaxial FePt thin film. Appl. Phys. Express *5*, 093002.

Murata, M., Nagase, K., Aoyama, K., and Yamamoto, A. (2020). Enhancement of figure of merit for Nernst effect in $Bi_{77}Sb_{23}$ alloy by Te-doping. Appl. Phys. Lett. *117*, 103903.

Nakamura, H., Hatano, N., and Shirasaki, R. (2005). Quantum Nernst effect. Solid State Commun. *135*, 510–514.

Nakamura, H., Ikeda, K., and Yamaguchi, S. (1997). Transport coefficients of InSb in a strong magnetic field. In Proceedings of the 16th International Conference on Thermoelectrics (IEEE), pp. 142–146.

Nakatsuji, S., Kiyohara, N., and Higo, T. (2015). Large anomalous Hall effect in a non-collinear antiferromagnet at room temperature. Nature *527*, 212–215.

Nakayama, H., Masuda, K., Wang, J., Miura, A., Uchida, K., Murata, M., and Sakuraba, Y. (2019). Mechanism of strong enhancement of anomalous Nernst effect in Fe by Ga substitution. Phys. Rev. Mater. *3*, 114412.

Nolas, G.S., Sharp, J., and Goldsmid, H.J. (2001). Thermoelectrics (Springer).

Norwood, M.H. (1963). Theory of Nernst generators and refrigerators. J. Appl. Phys. *34*, 594–599.

Ohta, M., Jood, P., Murata, M., Lee, C.-H., Yamamoto, A., and Obara, H. (2019). An integrated approach to thermoelectrics: combining phonon dynamics, nanoengineering, novel materials development, module fabrication, and metrology. Adv. Energy Mater. *9*, 1801304.

Reichlova, H., Schlitz, R., Beckert, S., Swekis, P., Markou, A., Chen, Y.C., Kriegner, D., Fabretti, S., Hyeon Park, G.H., Niemann, A., et al. (2018). Large anomalous Nernst effect in thin films of the Weyl semimetal Co_2MnGa. Appl. Phys. Lett. *113*, 212405.

Sakai, A., Minami, S., Koretsune, T., Chen, T., Higo, T., Wang, Y., Nomoto, T., Hirayama, M., Miwa, S., Nishio-Hamane, D., et al. (2020). Iron-based binary ferromagnets for transverse thermoelectric conversion. Nature *581*, 53–57.

Sakuraba, Y. (2016). Potential of thermoelectric power generation using anomalous Nernst effect in magnetic materials. Scr. Mater. *111*, 29–32.

Sakuraba, Y., Hasegawa, K., Mizuguchi, M., Kubota, T., Mizukami, S., Miyazaki, T., and Takanashi, K. (2013). Anomalous Nernst effect in $L1_0$-FePt/MnGa thermopiles for new thermoelectric applications. Appl. Phys. Express *6*, 033003.

Wang, Y., Li, L., and Ong, N.P. (2006). Nernst effect in high-T_c superconductors. Phys. Rev. B *73*, 024510.

Wolfe, R., and Smith, G.E. (1962). Effects of a magnetic field on the thermoelectric properties of a bismuth-antimony alloy. Appl. Phys. Lett. *1*, 5–7.

Xiang, J., Hu, S., Lyu, M., Zhu, W., Ma, C., Chen, Z., Steglich, F., Chen, G., and Sun, P. (2020). Large transverse thermoelectric figure of merit in a topological Dirac semimetal. Sci. China Phys. Mech. Astron. *63*, 237011.

Yamaguchi, S. (2002). Thermoelectric conversion and its application for nuclear fusion. J. Plasma Fusion Res. *78*, 19–35.

Yang, Z., Codecido, E.A., Marquez, J., Zheng, Y., Heremans, J.P., and Myers, R.C. (2017). Scalable Nernst thermoelectric power using a coiled galfenol wire. AIP Adv. *7*, 095017.

iScience, Volume *24*

Supplemental Information

Prototype fabrication and performance evaluation of a thermoelectric module operating with the Nernst effect

Masayuki Murata, Kazuo Nagase, Kayo Aoyama, Atsushi Yamamoto, and Yuya Sakuraba

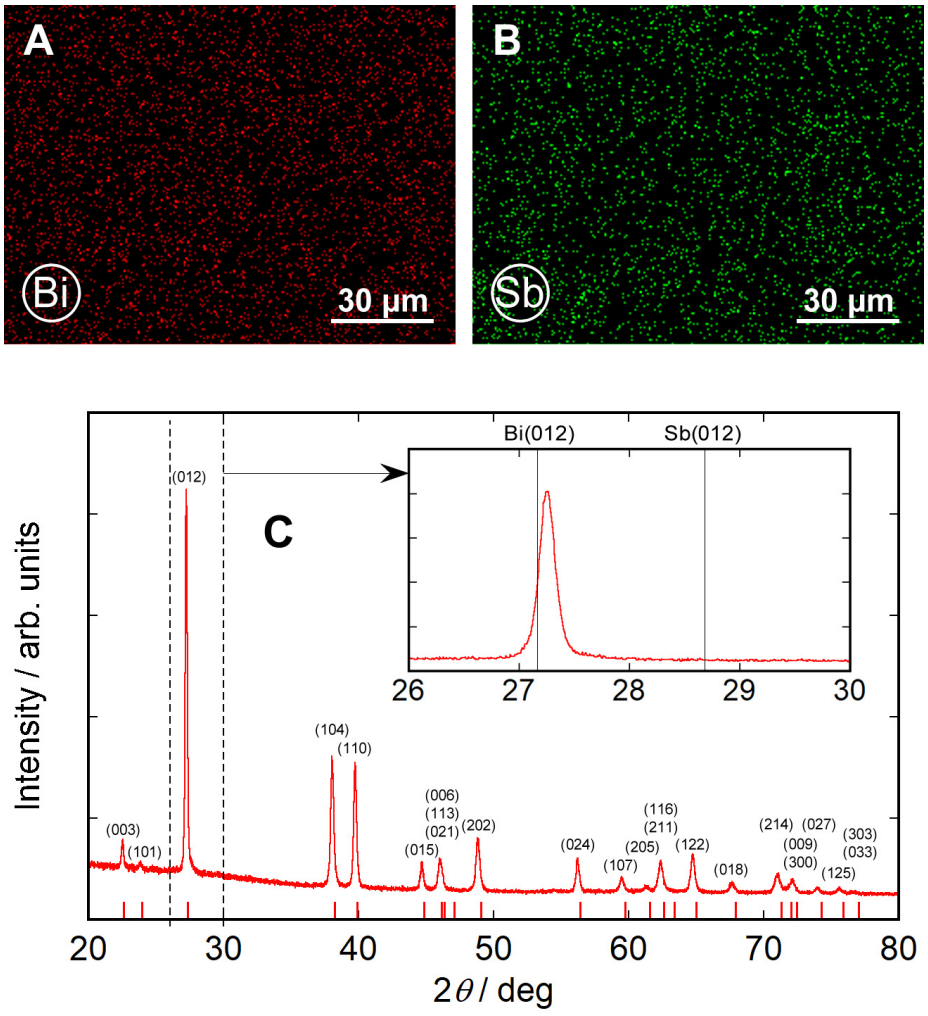

Figure S1. Analysis results of the prepared $Bi_{88}Sb_{12}$ sintered alloy, Related to Figure 2-3. EDX analysis maps of (A) Bi and (B) Sb. (C) X-ray diffraction pattern.

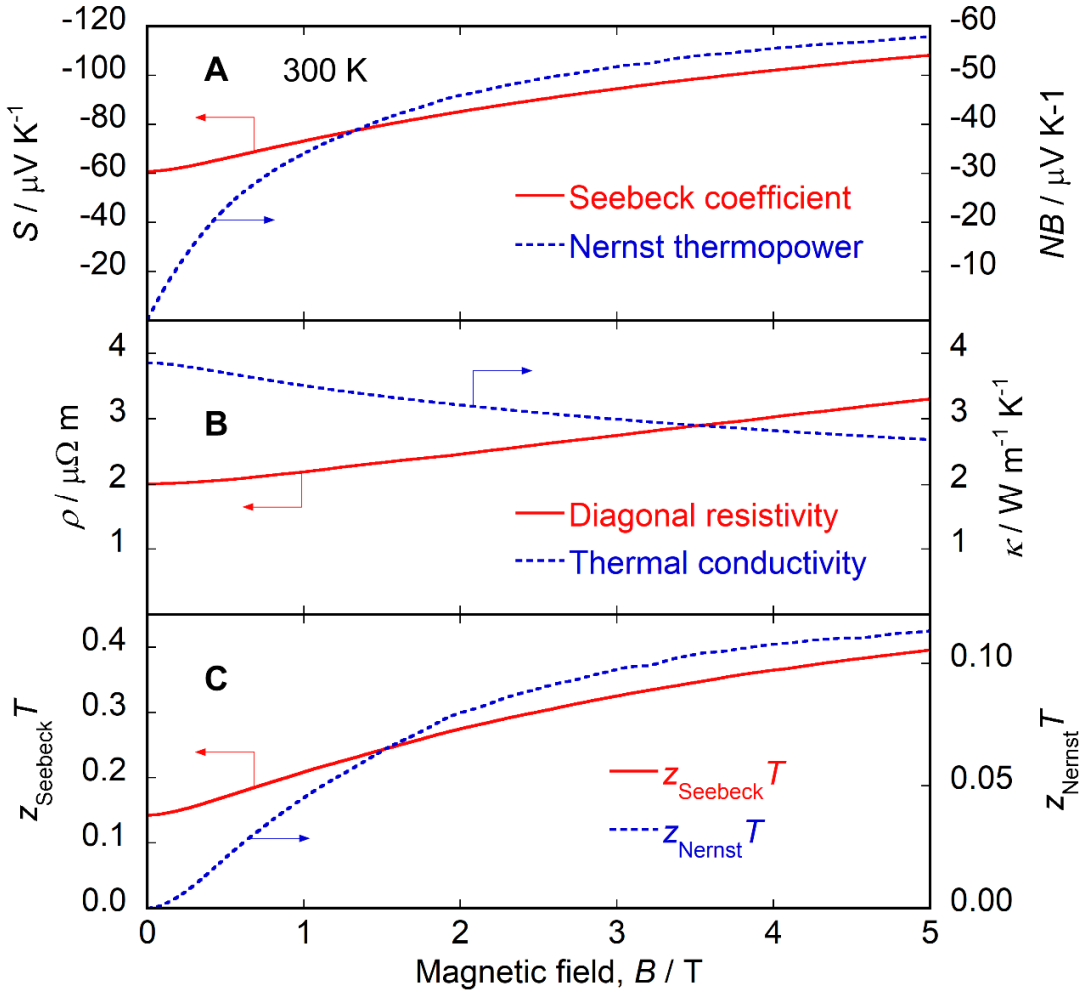

Figure S2. Measured magnetic field dependences of the thermomagnetic properties on the 0.06 at.% Te-doped $Bi_{88}Sb_{12}$ sintered alloy at 300 K, Related to Figure 2-3. (A) the Seebeck coefficient and Nernst thermopower, (B) electrical resistivity and thermal conductivity, (C) the dimensionless figure of merit for the Seebeck effect and for the Nernst effect.

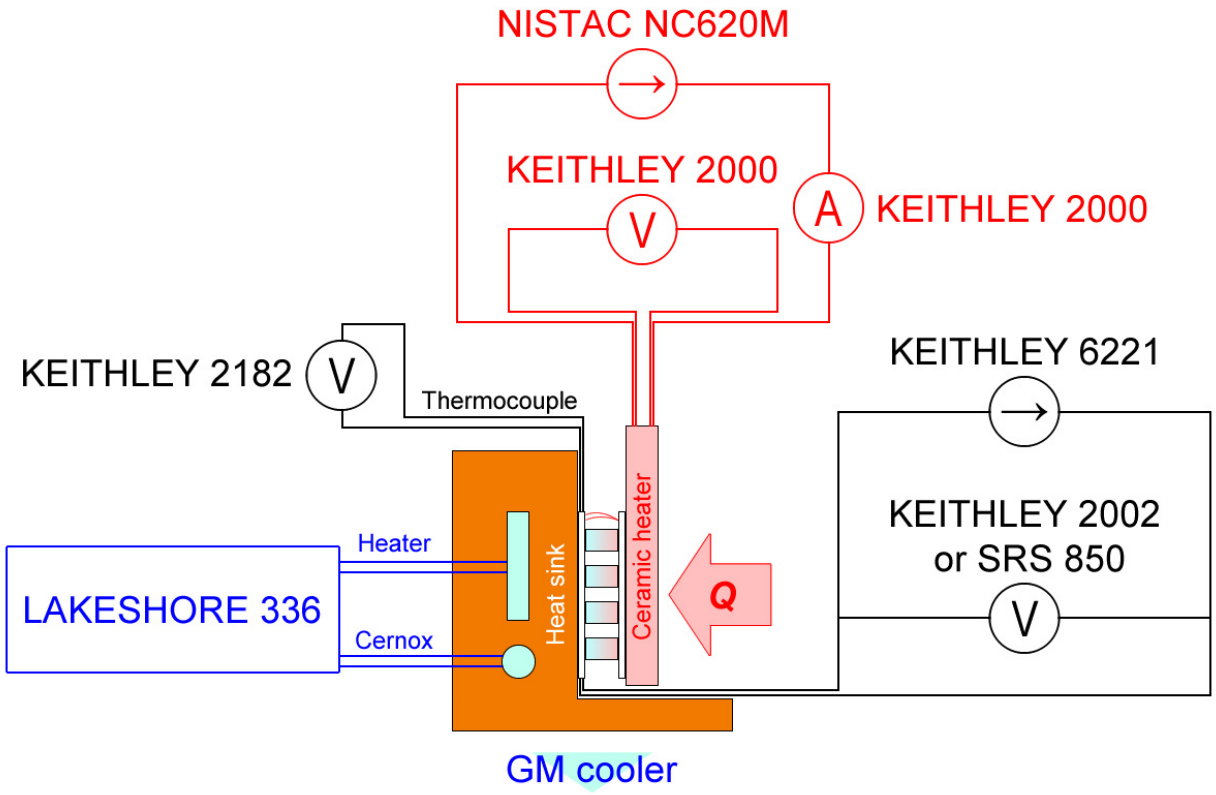

Figure S3. Schematic diagram of the equipment setup for the measurement of power generation and cooling on the Nernst-type thermoelectric module, Related to Figure 3.

TRANSPARENT METHODS

Material preparation

A polycrystalline $Bi_{88}Sb_{12}$ alloy was chosen as the material for the prototype of the Nernst-type thermoelectric module because a large Nernst coefficient has been reported for a Bi-Sb alloy of 12 at.% Sb in the room temperature range (Shabde, 1967). Bi and Sb of 99.99% purity shots, respectively, with an atomic ratio of 88:12, were placed inside a 250-ml agate jar, and ground by centrifugal ball milling (Retsch S100) using an agate ball 25 mm in diameter at 450 rpm for 60 min. The ground powder was sieved through a 38 μm mesh and 0.06 at.% Te powder (99.99% purity, <45 μm) is added because a small amount of Te-doping improves $z_{\mathrm{Nernst}}T$ (Murata et al., 2020). The powder was sintered at 220 °C and 50 MPa for 10 min under vacuum by the spark plasma sintering (SPS) method (Sumitomo Coal Mining SPS-515S) to produce cylindrical ingots with a diameter of 15 mm and thickness of approximately 3 mm. The sintered Bi-Sb ingot was annealed in vacuum-sealed quartz ampoules at 250 °C for 168 h, and the alloying of Bi and Sb was confirmed using energy dispersive X-ray (EDX) analysis (Hitachi High-Tech S-3500N), as shown in Figure S1(A,B) and X-ray diffraction (Rigaku SmartLab), as shown in Figure S1(C). In addition, EDX quantitative analysis confirmed that the atomic composition ratio of Bi and Sb was 87.6:12.4, which corresponds to the start composition.

The bar-shaped $Bi_{88}Sb_{12}$ alloys with dimensions of $2.03 \times 2.78 \times 7.36$ mm^3 were cut from the produced ingots and used for measuring the Seebeck and Nernst effect, diagonal resistivity and thermal conductivity. The magnetic field dependences of these properties of the $Bi_{88}Sb_{12}$ alloy were measured at

300 K using a cryostat equipped with a superconducting magnet (Cryogenic J1687). The measured magnetic field dependences of the Seebeck coefficient S, Nernst thermopower NB, electrical resistivity ρ, thermal conductivity κ, the dimensionless figure of merit for the Seebeck effect $z_{\mathrm{Seebeck}}T$, and for the Nernst effect $z_{\mathrm{Nernst}}T$ on the 0.06 at.% Te-doped $Bi_{88}Sb_{12}$ sintered alloy at 300 K are shown in Figure S2(A–C).

Measurement configuration

The schematic configuration of the measurement system of the Nernst-type thermoelectric module is shown in Figure S3. The output voltage and load current were measured when heat passed through the module from the ceramic heater to the heat sink, as shown in Figure S3. The heat sink temperature was controlled by a ceramic heater and Cernox thermometer operated by a temperature controller (Lakeshore 336). The hot side of the module was heated with a 1000-W rated ceramic heater using a power source (Nistac NC620M), and the input power was determined by the electrical current and voltage measured using two digital multimeters (DMM) (Keithley 2000). The temperature difference of the module was determined by the voltage of the differential thermocouple mounted inside the module measured by a nanovoltmeter (Keithley 2182) using the cold side temperature measured at the heat sink. The output power was determined by the voltage of the module measured by a digital multimeter (Keithley 2002) and the load current controlled by the current source (Keithley 6221). The internal resistance of the module was measured by the four-wire and alternating current measurement method at

an electrical current of 1 mA at a frequency of 11.234 Hz using a lock-in amplifier (Stanford Research Systems 860) and a Keithley 6221 current source. The module performance was evaluated in a magnetic field from −5 to 5 T, which was applied by the cryogen-free magnet system using a magnet power supply (Cryogenic SMS120 C).

As the Seebeck-type module generates a temperature difference due to the Peltier effect caused by the electrical current, the Nernst-type module generates a temperature difference due to the Ettingshausen effect. Therefore, we also attempt to demonstrate the Ettingshausen effect on the produced Nernst-type module at a magnetic field of 0 T, ±1 T, and ±5 T using the same configuration as the power generation characteristics. The temperature difference of the module was measured by a differential thermocouple when the electrical current flowed from −100 mA to +100 mA at 20-mA intervals.

SUPPLEMENTAL REFERENCES

Murata, M., Nagase, K., Aoyama, K., and Yamamoto, A. (2020). Enhancement of figure of merit for Nernst effect in $Bi_{77}Sb_{23}$ alloy by Te-doping. Appl. Phys. Lett. *117*, 103903.

Shabde, S.N. (1967). The hall and Nernst effect in Bi and *Bi*-Sb alloys, Rice University Ph.D. thesis.